

# Thermal decomposition of $\text{Mo}(\text{CO})_6$ on thin $\text{Al}_2\text{O}_3$ film: A combinatorial investigation by XPS and UPS

Zhiquan Jiang<sup>a,b</sup>, Weixin Huang<sup>b</sup>, Zhen Zhang<sup>a</sup>, Hong Zhao<sup>a</sup>, Dali Tan<sup>a</sup>, Xinhe Bao<sup>a,\*</sup>

<sup>a</sup> State Key Laboratory of Catalysis, Dalian Institute of Chemical Physics, Chinese Academy of Sciences, Dalian 116023, China

<sup>b</sup> Department of Chemical Physics, University of Science and Technology of China, Hefei 230026, China

Received 16 August 2006; accepted for publication 13 November 2006

Available online 1 December 2006

## Abstract

A thin and homogeneous alumina film was prepared by deposition and oxidation of aluminum on a refractory Re(0001) substrate under ultrahigh vacuum conditions. X-ray photoelectron spectroscopy (XPS), ultraviolet photoelectron spectroscopy (UPS) and high-resolution electron-energy-loss spectroscopy (HREELS) demonstrate that the oxide film is long-range ordered, essentially stoichiometric and free from surface hydroxyl groups. The chemisorption and thermal decomposition of  $\text{Mo}(\text{CO})_6$  on the  $\text{Al}_2\text{O}_3$  film were investigated by means of XPS and UPS.  $\text{Mo}(\text{CO})_6$  adsorbs molecularly on the oxide film at 100 K; however, thermal decomposition of the adsorbate occurs upon annealing at high temperatures. Consequently the metallic molybdenum clusters are deposited on the thin alumina film via complete decarbonylation of  $\text{Mo}(\text{CO})_6$ .

© 2006 Elsevier B.V. All rights reserved.

**Keywords:** Molybdenum hexacarbonyl; Thin  $\text{Al}_2\text{O}_3$  film; Thermal decomposition; X-ray photoelectron spectroscopy; Ultraviolet photoelectron spectroscopy

## 1. Introduction

The adsorptive and reactive properties of organometallic compounds on catalyst surfaces have recently attracted increasing attention. Group VIB hexacarbonyls render themselves suitable as precursors for selective metal deposition on the surfaces, to provide an effective route in the preparation of supported metal catalysts [1]. The metals in the carbonyls are normally in the zero-valent state and the CO ligands are by themselves a stable, noncondensable gas, so that thermal decomposition of metal carbonyls can, in principle, eliminate CO from the carbonyl molecules, leaving the metal on the surface.

Alumina-supported molybdenum and molybdenum oxide catalysts are well-known in a variety of applications: metathesis of alkenes, hydrodesulfurization, hydrogenation,

to mention few. Usually such catalysts are obtained by wet impregnation of alumina by a molybdenum salt, but as early as 1964 [2] it was shown that molybdenum-supported catalysts active for olefin metathesis could be prepared via adsorption of  $\text{Mo}(\text{CO})_6$  on  $\gamma$ -alumina followed by appropriate activation. The reaction of molybdenum hexacarbonyl with alumina is extensively used to synthesize active catalysts for a range of reactions including alkene hydrogenation and olefin metathesis, where the activity for a particular reaction depends on the pretreatment conditions [3–6]. The adsorption and reaction of molybdenum hexacarbonyl on  $\gamma$ -alumina has been studied by means of various techniques, including infrared spectroscopy, thermal desorption spectroscopy, X-ray photoelectron spectroscopy and nuclear magnetic resonance, and the formation of different subcarbonyl species was observed on the oxide surface [7–10].

In recent years, significant progress has been made in growing and characterizing thin oxide films as supports for model catalysts. It has been shown that oxide films

\* Corresponding author. Tel.: +86 411 84686637; fax: +86 411 84694447.  
E-mail address: [xhbao@dicp.ac.cn](mailto:xhbao@dicp.ac.cn) (X. Bao).

grown on refractory metal surfaces can successfully mimic the properties of the conventional high-surface-area oxides widely used as supports in catalysis. This approach offers the advantage of using the full range of ultrahigh vacuum (UHV) surface analytical techniques to scrutinize the surface chemistry, while avoiding the charging problems that would normally occur when electron-based techniques are used with insulating samples. The interaction between  $\text{Mo}(\text{CO})_6$  and alumina thin films has been studied at low temperatures under UHV conditions [11–18], in order to mimic the real catalyst systems. It was reported that  $\text{Mo}(\text{CO})_6$  desorbed molecularly from the surface below  $\sim 250$  K and also reacted to form strongly bound species, where these reaction pathways competed [11,14]. In addition, reaction of low exposures of  $\text{Mo}(\text{CO})_6$  with alumina films above 500 K resulted in the formation of nanoparticles on the surface, while higher exposures (of  $\sim 5000$  L of  $\text{Mo}(\text{CO})_6$ ) led to a thin film that completely covered the substrate [16].

In a preceding paper [19] metallic molybdenum was observed to be deposited on fully dehydroxylated alumina film via thermal decomposition of  $\text{Mo}(\text{CO})_6$  and subsequent annealing at high temperatures. To the best of our knowledge, the detailed XPS and UPS results are not reported about  $\text{Mo}(\text{CO})_6$  decomposition on the thin  $\text{Al}_2\text{O}_3$  film. In order to further address the detail for the decarbonylation process of  $\text{Mo}(\text{CO})_6$  on the thin  $\text{Al}_2\text{O}_3$  film upon annealing, we present in the following the results on the thermal decomposition of  $\text{Mo}(\text{CO})_6$  by means of XPS and UPS. To the best of our knowledge, the detailed XPS and UPS evidences are not reported about  $\text{Mo}(\text{CO})_6$  decomposition on the thin  $\text{Al}_2\text{O}_3$  film. In another paper CO chemisorption on the metallic molybdenum nanoparticles, which were deposited on the thin  $\text{Al}_2\text{O}_3$  film via an electron-beam assisted evaporator, was investigated by XPS and UPS [20]. In comparison with the XPS and UPS results of  $\text{Mo}(\text{CO})_6$  chemisorption on the thin  $\text{Al}_2\text{O}_3$  film, it is deduced that a binary compound of molybdenum and CO is formed on the surface upon CO dose, accompanied with a positive binding energy shift of the Mo 3d doublet and a localized Mo 4d valence band. This observation is in good accordance with the TDS results on the metallic molybdenum nanoparticles in [21]. The formation of the  $\text{Mo}_x(\text{CO})_y$  species implies that the property of the metallic molybdenum nanoparticles on the thin alumina film is much different from that of the bulk molybdenum, indicating a significant nanometer size effect.

## 2. Experimental

Experiments were performed on an Omicron multiprobe surface analysis system with a base pressure of below  $2.0 \times 10^{-10}$  mbar. The system consists of three ultrahigh vacuum chambers: preparation, characterization and SPM chambers. The preparation chamber is equipped with evaporators for aluminum and molybdenum, and an ion-sputtering gun for sample cleaning. The SPM chamber is

mainly for scanning tunneling microscopy/atomic force microscopy (STM/AFM, Omicron VT Beam Deflection AFM) observation. The characterization chamber is equipped with facilities for X-ray photoelectron spectroscopy (XPS) and ultraviolet photoelectron spectroscopy (UPS), a LK-ELS5000 instrument for high-resolution electron energy-loss spectroscopy (HREELS). XPS data were collected by Mg  $K\alpha$  radiation ( $h\nu = 1253.6$  eV) with a power of 300 W. All UP spectra were recorded at detection angles perpendicular to the sample surface with He I radiation ( $h\nu = 21.2$  eV), and the photoelectron peak positions were referenced to the Fermi level of the clean Re(0001) substrate. The HREEL spectra were taken in the specular direction with an incident angle of  $60^\circ$ , primary incident electron-beam energy of 7.287 eV and a typical energy resolution of 5–8 meV on the metallic substrate. The three chambers are connected with a transfer chamber, through which the sample can be transferred between these three chambers by magnetically coupled probes without breaking the vacuum.

A Re(0001) single crystal was mounted on an Omicron sample holder and resistively heated by a PBN heater. The sample temperature was monitored by a chromel–alumel thermocouple spot-welded on the back side of the metallic substrate. The sample was cleaned by standard procedures, including oxidation,  $\text{Ar}^+$  ion-sputtering and annealing at a high-temperature, until no contaminants could be detected by XPS. A homemade aluminum evaporator was used to prepare the thin  $\text{Al}_2\text{O}_3$  film. An aluminum oxide film formed on the refractory Re(0001) substrate by depositing aluminum in an oxygen atmosphere of  $3.0 \times 10^{-6}$  mbar at room temperature and then annealing up to 1200 K.  $\text{Mo}(\text{CO})_6$ , further purified by several freeze-pump-thaw cycles, was introduced onto the sample surface by backfilling the chamber. All exposures were specified hereafter as Langmuirs ( $1 \text{ L} = 1.0 \times 10^{-6}$  Torr s).

## 3. Results and discussion

An aluminum oxide film formed by depositing aluminum onto a clean Re(0001) substrate at room temperature in  $3.0 \times 10^{-6}$  mbar of oxygen. Fig. 1 shows XPS of the thin oxide film annealed at the indicated temperatures after deposition at room temperature. When the aluminum oxide film was deposited onto the Re(0001) substrate, XPS exhibits Al 2s signal at 121.2 eV and O 1s signal at 533.1 eV, while no feature associated with the Re substrate is observed over the entire energy range. The Al 2s and O 1s XPS peaks remain unchanged with increasing sample temperature. When the sample was annealed at 800 K, these two signals both shift toward lower binding energy, with values of 120.7 and 532.5 eV, respectively upon annealing at 1000 K. When the sample temperature was increased to 1200 K, the Al 2s and O 1s XPS peaks settle at 120.8 and 532.6 eV, respectively. These two peaks are in line with the results of  $\text{Al}_2\text{O}_3$  film deposited on Re(0001) substrate [22]. However, the Al 2s and O 1s signals both

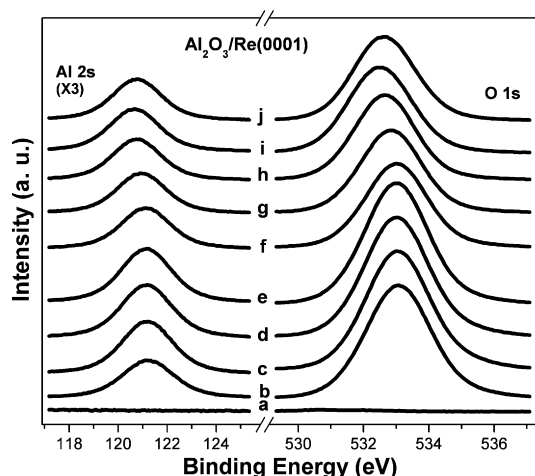


Fig. 1. XPS of the  $\text{Al}_2\text{O}_3$  thin film annealed at the indicated temperatures. (a) a clean  $\text{Re}(0001)$  substrate; after the deposition of thin oxide film at room temperature, the sample was annealed at (b) 300 K, (c) 400 K, (d) 500 K, (e) 600 K, (f) 700 K, (g) 800 K, (h) 900 K, (i) 1000 K, (j) 1200 K.

shift downward in binding energy with increasing substrate temperature, compared to the initial situation at room temperature. It should be mentioned that static charging on the film should not be a major factor for the downward shifts of the Al 2s and O 1s signals. HREEL spectra (Fig. 2) of the oxide film provide sufficient evidence that static charging is not a problem in our investigation. The simultaneous negative binding energy shifts of the Al 2s and O 1s signals are due to the final-state effect. The oxygen atoms undergo migration and redistribution within the thin film upon annealing, inducing the oxide film to be well-ordered.

In our experiments, the aluminum evaporated onto Re substrate in an oxygen ambient is expected to be com-

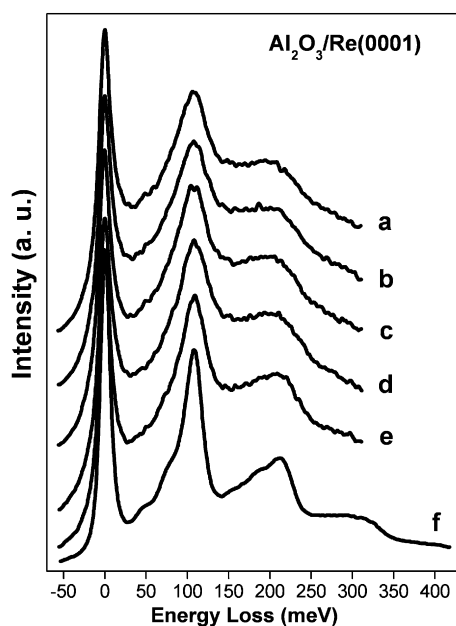


Fig. 2. HREELS of the thin aluminum oxide film annealed at (a) 300 K, (b) 500 K, (c) 700 K, (d) 800 K, (e) 1000 K, (f) 1200 K after deposition at room temperature.

pletely oxidized, even though the oxygen pressure is as low as  $3.0 \times 10^{-6}$  mbar. The main thermodynamic factors that may compete with the oxidation of film and substrate are related to the exothermic alloying between Al and substrate. However, the heat of formation of Al–Re alloy is on the order of  $-50$  kJ/mol [23], much smaller than that of aluminum oxide (on the order of  $-1600$  kJ/mol [24]). Therefore oxide formation should dominate over alloy formation. The oxide film is estimated to be at least 10 nm thick, based on that no contribution from the Re substrate is observed in XPS measurements. Taking into consideration the sensitivity factor, the thin oxide film is estimated to be stoichiometric according to the formula in [22]. Additionally, the stoichiometry of the acquired oxide film can also be deduced from the core level binding energies of the Al 2s and O 1s peaks.

The increase of the order within the thin  $\text{Al}_2\text{O}_3$  film upon annealing at high temperatures is also evidenced by means of HREELS, as shown in Fig. 2. After deposition at room temperature, a strong peak appears at 107 meV on the thin film, and another feature at 210 meV as a double phonon loss. These two features both slightly intensify with increasing sample temperature. When the sample was annealed at 1200 K, three distinguishable vibrational peaks emerge at 48, 79, and 108 meV, respectively, and their double and combinative phonon losses extend up to 220 meV. It is worth mentioning that a wide feature extending up to 315 meV is also obviously present in the HREEL spectrum, due to the triple and combinative phonon losses. The emergence of these phonon losses indicates that the obtained  $\text{Al}_2\text{O}_3$  film is highly ordered, in good agreement with the results of thin oxide films on  $\text{NiAl}(110)$  and  $\text{Ru}(0001)$  substrates [25]. Each of the three main loss features can be assigned to the octahedral and tetrahedral  $\text{Al}^{3+}$  occupation in crystalline  $\text{Al}_2\text{O}_3$  films. The 108 meV loss feature is due to a group of microscopic stretching motions between the octahedrally coordinated  $\text{Al}^{3+}$  cation and its six nearest-neighbouring  $\text{O}^{2-}$  anions, the 79 meV loss feature is due to a group of stretching motions between the tetrahedrally coordinated  $\text{Al}^{3+}$  cation and its four nearest-neighbouring  $\text{O}^{2-}$  anions, and the 48 meV loss feature is due to a vertical stretching motion of the subsequent in-phase O–Al planes. Therefore, a clear observation of the loss feature at 48 meV can be a sign for the vertically well-defined crystalline  $\text{Al}_2\text{O}_3$  films. It has been suggested that the appearance of the two phonon modes were characteristic of very thin  $\text{Al}_2\text{O}_3$  film [26]. Wu and Goodman [27] also found that the surface optical phonon losses of the thin  $\text{Al}_2\text{O}_3$  film were characterized by a two-mode pattern, whereas three modes of the phonon losses were typical for the thick film. Long-range order of the oxide film is achieved by depositing aluminum in ambient oxygen and subsequent annealing at elevated temperatures, as illustrated by the reinforcement of the vibrational features. HREELS results also demonstrate that this thin oxide film is free from surface hydroxyl groups, since it is prepared under UHV conditions.

Fig. 3 shows the valence band spectra (He I radiation) of the thin  $\text{Al}_2\text{O}_3$  film annealed at elevated temperatures after deposition at room temperature. Good UP spectrum is acquired on the clean  $\text{Re}(0001)$  substrate, similar to the results in literature [28], and then all UP spectra reported here are referenced to the Fermi level of the clean  $\text{Re}(0001)$  substrate. When  $\text{Al}_2\text{O}_3$  was deposited on the metallic substrate at room temperature, a strong emission from the O 2p-derived valence band shows a maximum intensity at around 7.9 eV. There is no observable change in the UP spectra in the initial stage of annealing at elevated temperatures. Further increasing substrate temperature, a distinguishable change is detected in the UP spectra. When the sample was annealed at 1000 K, the feature of O 2p valence band obviously increases its intensity, and simultaneously shifts toward lower binding energy. A distinct cleavage occurs on the O 2p-derived feature, with a primary peak at 6.9 eV, and two shoulder peaks at 9.3 and 11.4 eV below the Fermi level. This split of the line shape is assigned to hybridization of Al(3s-p) and O(2p) valence bands [29]. Upon oxidation of the Al(111) surface by  $10^6$  L of oxygen, two maxima in the  $\text{Al}_2\text{O}_3$  valence band were observed at 7.6 and 11.2 eV below the Fermi level, the former being attributed to non-bonding 2p lone pair orbitals and the latter to the hybridized oxygen  $\text{sp}^2$  orbitals mixed with the aluminum  $\text{sp}^3$  orbitals [30]. It indicates that the strong bonding happens between the aluminum and the oxygen upon annealing at elevated temperatures. When the sample temperature was raised up to 1200 K, the band intensity further rises and the feature continues to shift downward in binding energy, while the cleavage of the valence band grows more distinct. The valence band feature

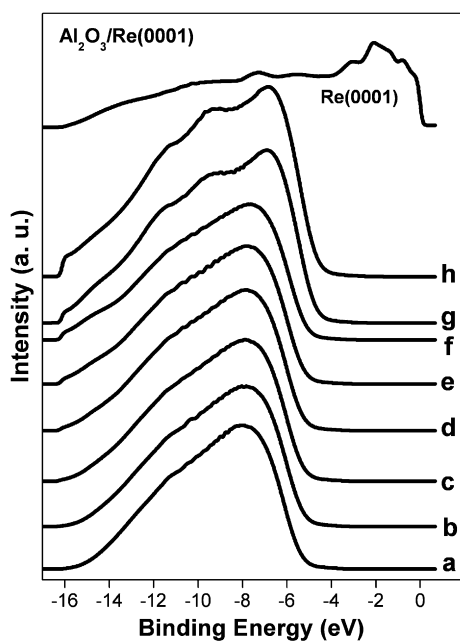


Fig. 3. UPS of the thin aluminum oxide film annealed at (a) 300 K, (b) 500 K, (c) 600 K, (d) 700 K, (e) 800 K, (f) 900 K, (g) 1000 K, (h) 1200 K after deposition at room temperature.

acquired on the thin oxide film is similar to that of  $\gamma\text{-Al}_2\text{O}_3$  [31], indicating that this aluminum oxide film after high-temperature annealing is characteristic of  $\gamma\text{-Al}_2\text{O}_3$ . A gradual transition from amorphous aluminum oxide to crystalline  $\gamma\text{-Al}_2\text{O}_3$  with increasing oxidation temperature was also observed in the case of thermal oxidation of a bare Al(431) substrate [32]. The characteristic of  $\gamma\text{-Al}_2\text{O}_3$  on the acquired oxide film is also confirmed by the vibrational feature in HREELS, since calculation of  $\gamma\text{-Al}_2\text{O}_3$  surfaces suggested that three strong phonon losses should appear at 400, 658, and 909  $\text{cm}^{-1}$  [33], while  $\alpha\text{-Al}_2\text{O}_3$  exhibited two strong fundamental vibrational modes at 496 and 806  $\text{cm}^{-1}$  [34].

$\text{Mo}(\text{CO})_6$  chemisorption on the thin  $\text{Al}_2\text{O}_3$  film was investigated by means of HREELS, as shown in Fig. 4. When the  $\text{Al}_2\text{O}_3$  film was exposed to 10 L  $\text{Mo}(\text{CO})_6$  at 100 K, the adsorption layer of the adsorbates suppresses the vibrational signal of the oxide film, inducing the 108 meV peak to decrease its intensity. New intense vibrational features are observed at 48, 75, and 250 meV upon  $\text{Mo}(\text{CO})_6$  chemisorption. These peaks are attributed to the Mo–CO stretch ( $\nu_8$ ), Mo–CO bend ( $\nu_7$ ) and C–O stretch ( $\nu_6$ ), respectively, in accordance with the vibrational modes for  $\text{Mo}(\text{CO})_6$  molecules in the gas phase [35–37]. The energies of these peaks are in good agreement with those observed on Rh(100) [38], Cu(111) [39], graphite and Ag(111) [40] surfaces by HREELS. In addition, a number of low intensity peaks resolved on the surface exposed to 10 L  $\text{Mo}(\text{CO})_6$  can also be well explained by the vibrational modes of  $\text{Mo}(\text{CO})_6$  molecules. The peaks at 150, 296, 324, and 353 meV are assigned to combination modes of  $2\nu_7$ ,  $\nu_6 + \nu_8$ ,  $\nu_6 + \nu_7$ , and  $\nu_6 + 2\nu_8$  of  $\text{Mo}(\text{CO})_6$ , respectively. The observation of combinative and multiple phonon

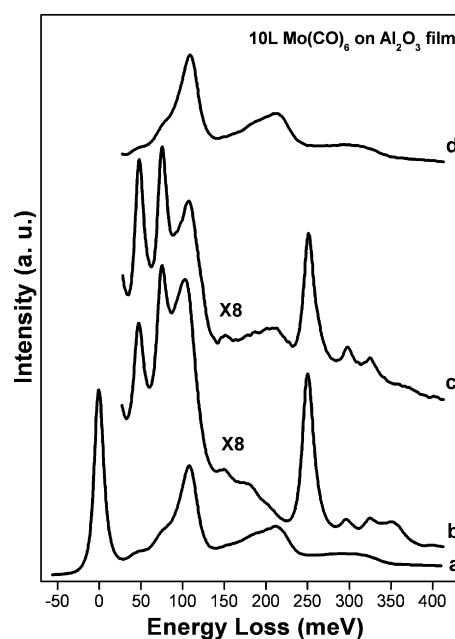


Fig. 4. HREELS of (a) the thin  $\text{Al}_2\text{O}_3$  film, and the sample annealed at (b) 100 K, (c) 150 K, (d) 200 K after dose of 10 L  $\text{Mo}(\text{CO})_6$  at 100 K.

losses suggests that a thick physically-adsorbed layer of  $\text{Mo}(\text{CO})_6$  forms on the thin  $\text{Al}_2\text{O}_3$  film. With annealing the sample at 150 K, the combinative phonon loss at 353 meV disappears, and the feature due to the multiple phonon losses of the oxide film emerges again in the HREEL spectrum. This implies that part of the adsorbates desorb from the surface at 150 K. When the sample temperature is increased up to 200 K, there is no observable vibrational signal on the surface corresponding to the adsorbed  $\text{Mo}(\text{CO})_6$  molecules, only the vibrational features related with the oxide film. This illustrates that most of the  $\text{Mo}(\text{CO})_6$  adsorbates have already desorbed from the surface upon 200 K annealing, in excellent agreement with the TDS results of  $\text{Mo}(\text{CO})_6$  on the thin alumina film [19]. Henceforth thermal decomposition of the residual  $\text{Mo}(\text{CO})_6$  occurs with increasing substrate temperature.

Fig. 5 shows Mo 3d XPS of  $\text{Mo}(\text{CO})_6$  on the  $\text{Al}_2\text{O}_3$  thin film as a function of substrate temperature. When 10 L  $\text{Mo}(\text{CO})_6$  was dosed onto the oxide film, a Mo 3d doublet appears at 229.2 and 232.4 eV in XP spectrum, corresponding to molecularly adsorbed  $\text{Mo}(\text{CO})_6$  species. These two peaks shift toward lower binding energy with increasing sample temperature, indicating partial thermal decomposition of the adsorbates upon annealing. Simultaneously the Mo 3d XPS signal slightly decreases its intensity, implying that desorption of  $\text{Mo}(\text{CO})_6$  also occurs during the heating process. As is mentioned in the preceding paper [19], the heating rate plays a very important role on the ratio between desorption and decomposition of the adsorbed  $\text{Mo}(\text{CO})_6$  species upon annealing. The negative binding energy shift of the Mo 3d doublet is due to the formation of

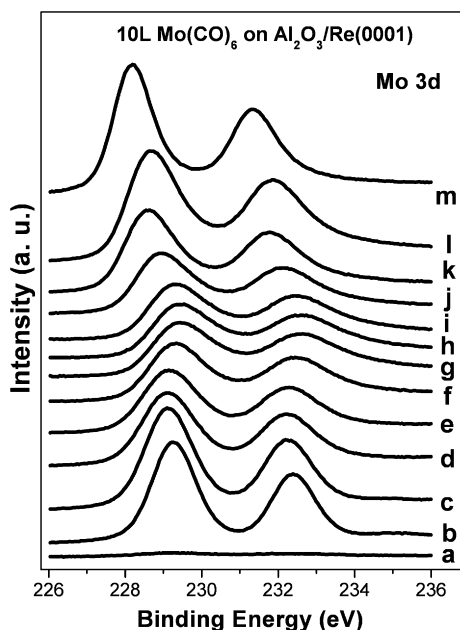


Fig. 5. Mo 3d XPS of  $\text{Mo}(\text{CO})_6$  adsorbed on the thin  $\text{Al}_2\text{O}_3$  film, (a) a clean  $\text{Al}_2\text{O}_3$  film; After dose of 10 L  $\text{Mo}(\text{CO})_6$  on the  $\text{Al}_2\text{O}_3$  film at 100 K, the sample was annealed at (b) 100 K, (c) 150 K, (d) 200 K, (e) 250 K, (f) 300 K, (g) 400 K, (h) 500 K, (i) 600 K, (j) 700 K, (k) 800 K, (l) 900 K, (m) 1000 K.

molybdenum subcarbonyls species derived from partial decomposition. Cho and Bernasek [41] also observed similar phenomena when they used wide-band UV radiation from a mercury lamp to irradiate the adsorbed  $\text{Mo}(\text{CO})_6$  layers. The Mo  $3d_{5/2}$  peak locates at 229.0 eV with substrate temperature of 200 K. Further increasing sample temperature, Mo 3d peaks shift toward higher binding energy. Extensive dissociation of the surface molybdenum subcarbonyls occurs, which converts subcarbonyls into the metallic molybdenum. The Mo  $3d_{5/2}$  peak reaches its maximal binding energy of 229.4 eV upon 500 K annealing. It indicates that molybdenum subcarbonyls have already completed decarbonylation at 500 K, also in coincidence with the TDS results of  $\text{Mo}(\text{CO})_6$  on the thin alumina film [19]. The molybdenum is well dispersed on the oxide film in the metallic form. When the sample was heated at higher temperatures, the Mo 3d doublet shifts downward in binding energy again, at 228.2 eV upon 1000 K annealing. This negative binding energy shift, as observed on the Mo/ $\text{Al}_2\text{O}_3$  model catalysts at elevated temperatures [19], is due to aggregation of the metallic molybdenum, which causes the particle size to increase. In the case of molybdenum deposition on a stoichiometric  $\text{TiO}_2(110)$  surface [42], Mo 3d XPS peaks were observed to shift with varying coverages, from 228.7 eV at 0.15 equivalent ML to 227.6 eV at 3.2 equivalent ML.

Fig. 6 shows C 1s and O 1s XPS of  $\text{Mo}(\text{CO})_6$  on the  $\text{Al}_2\text{O}_3$  thin film as a function of substrate temperature. When the film was exposed to 10 L  $\text{Mo}(\text{CO})_6$  at 100 K, a prominent feature appears at 287.8 eV in the C 1s region, with a smaller peak at 293.3 eV. The former is attributed to the photoemission of molybdenum hexacarbonyl and subcarbonyls adsorbed on the surface, while the latter to the corresponding intense shake-up satellites in the C 1s

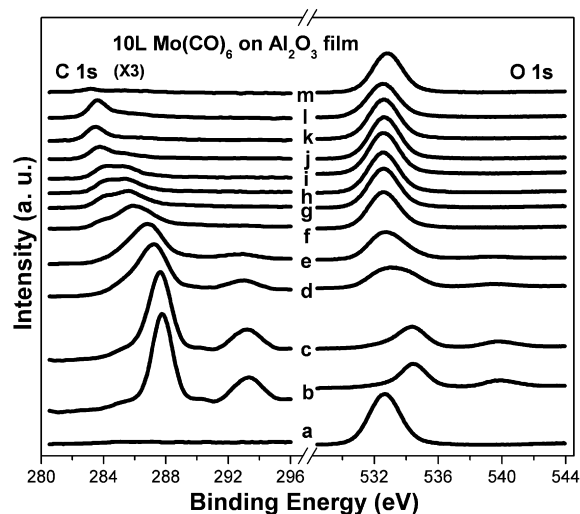


Fig. 6. C 1s and O 1s XPS of  $\text{Mo}(\text{CO})_6$  adsorbed on the thin  $\text{Al}_2\text{O}_3$  film, (a) a clean  $\text{Al}_2\text{O}_3$  film; After dose of 10 L  $\text{Mo}(\text{CO})_6$  on the  $\text{Al}_2\text{O}_3$  film at 100 K, the sample was annealed at (b) 100 K, (c) 150 K, (d) 200 K, (e) 250 K, (f) 300 K, (g) 400 K, (h) 500 K, (i) 600 K, (j) 700 K, (k) 800 K, (l) 900 K, (m) 1000 K.

region. In the metal carbonyl complex the electron structure can be described by a set of symmetry adapted orbitals of octahedral symmetry, and accordingly the symmetry of the CO orbitals and metal orbitals has to be reduced to the correct point group. Transition metal carbonyls show evidence of strong multielectron excitations following core ionization manifested in their photoelectron spectra by shake-up satellite lines. The intensities of the individual shake-up processes are normally low compared to the main line of the spectrum. However, in some systems, where a large gain in relaxation energy is obtained by charge transfer within the molecule, shake-up satellites appear with large intensities comparable to the main line [43,44]. Moreover, the satellite spectrum changes considerably in intensity when the molecules are condensed into solids due to the appearance of intermolecular screening of the core hole. The O 1s region also exhibits electronic structure of intense shake-up satellites, a primary feature at 534.5 eV and a satellite peak at 539.9 eV. The thick adsorption layer of Mo(CO)<sub>6</sub> inhibits the photoemission of the oxide film in the O 1s region. Similar intense satellites in the C 1s and O 1s spectra have been found in other metal carbonyls [43–46]. These core shake-up spectra could be assigned using  $Z + 1$  approximation, considering the charge transfer from the metal to the ligand in which the core ionization process took place [43].

When the Mo(CO)<sub>6</sub> adsorption layer was heated, the features of C 1s and O 1s XPS signals move toward lower binding energy, and gradually decrease their intensities with the substrate temperature. The negative binding energy shift and gradual intensity decrease of XPS signals both indicate that the adsorbed molecules undergo desorption and thermal decomposition, as informed by the change of the Mo 3d doublet upon annealing. When the sample temperature was raised up to 300 K, the satellite peak in the C 1s region disappears, while another feature is still visible at 286.8 eV. This indicates that thermal decomposition takes place on the residual molybdenum subcarbonyls. Further increasing substrate temperature, the C 1s peak continues to shift downward in binding energy and to reduce its intensity. In particular, a new feature for C 1s photoemission develops at 284.2 eV. This new peak increases monotonically its intensity, which is of the same order of magnitude with another XPS peak at the substrate temperature of 600 K. This new feature is due to the photoemission of the carbon deposits on the surface, which is derived from the dissociation of CO in the presence of the metallic molybdenum particles. The deposited carbon species due to CO dissociation was also observed by means of Auger electron spectroscopy [19]. Only one peak at 283.7 eV is visible in the C 1s spectra upon further annealing, and it keeps on moving toward lower binding energy with the sample temperature. It implies that under the effect of high-temperature, the carbon species and the metallic molybdenum interact strongly, and then the molybdenum carbide species form on the surface, inducing the C 1s feature to shift downward in binding energy.

When the sample was annealed at 1000 K, no C 1s feature is detected on the surface, indicating the formed molybdenum carbide species has been reduced by the oxygen contained in the thin Al<sub>2</sub>O<sub>3</sub> film. Due to the strong O 1s interference from the oxide film, the change of the O 1s region is obscured upon annealing, with the exception of desorption and thermal decomposition of the adsorbed Mo(CO)<sub>6</sub>.

Thermal decomposition of Mo(CO)<sub>6</sub> was also investigated by means of UPS, illustrated in Fig. 7 as a function of the substrate temperature. The difference spectra shown in the right panel were obtained by subtracting the spectrum on the surface annealed at the indicated temperatures from the initial spectrum (a) of the clean Al<sub>2</sub>O<sub>3</sub> film. When 10 L Mo(CO)<sub>6</sub> was dosed on the thin film at 100 K, two prominent features appear at 14.7 and 10.7 eV in the UPS. As reference to the valence band spectra of Mo(CO)<sub>6</sub> in gas phase [47,48], these two features are assigned to the characteristic photoemission of the carbonyl ligands,  $4\sigma$  and  $1\pi + 5\sigma$  orbitals, respectively. UPS [48] and electron-impact ionization studies [49] revealed that the  $5\sigma/1\pi$  and  $4\sigma$  levels of gas phase Mo(CO)<sub>6</sub> were at 13.9 and 17.9 eV, respectively; while the  $5\sigma$ ,  $1\pi$ , and  $4\sigma$  levels of solid Mo(CO)<sub>6</sub> were observed at 11.9, 13.5, and 16.5 eV, respectively [48]. There are two negative peaks at 11.2 and 6.4 eV in the difference spectrum, derived from the inhibition and suppression of the valence band emission from the thin Al<sub>2</sub>O<sub>3</sub> film by the thick adsorption layer of Mo(CO)<sub>6</sub>. With increasing sample temperature, the valence band emission of the carbonyl ligands shifts toward lower binding energy and reduces the intensity. This suggests that thermal decomposition of the adsorbed Mo(CO)<sub>6</sub> occurs and the molybdenum subcarbonyls form on the oxide film upon annealing. Simultaneously, the intensity of the negative peaks in the right panel decreases, illustrating that the thickness of the adsorption layer reduces and the suppression of the photoemission of the oxide substrate is weakened.

For detailed investigation we focus on the change of the valence band emission upon Mo(CO)<sub>6</sub> chemisorption on the thin Al<sub>2</sub>O<sub>3</sub> film in the binding energy region between 0 and 5 eV, as shown in Fig. 8. When the oxide film was exposed to 10 L Mo(CO)<sub>6</sub> at 100 K, an obvious feature appears at 3.9 eV, due to the photoemission of the Mo 4d valence band in the adsorbed Mo(CO)<sub>6</sub>. UPS [48] and electron-impact ionization studies [49] revealed that the 4d level of gas phase Mo(CO)<sub>6</sub> was at 8.4 eV; while that of solid Mo(CO)<sub>6</sub> was observed at 7.1 eV using photon radiation at 40.8 eV [48]. For Mo(CO)<sub>6</sub> physisorbed on Si(111)-7×7, the highest occupied molecular orbital (HOMO) (4d) and the lowest unoccupied molecular orbital (LUMO) (4d\*) were 7 and 3.2 eV, respectively, below the vacuum level [50,51]. Taking into account the separation between the vacuum level and the Fermi level, the binding energy of the Mo 4d valence band in our case is in good agreement with that in solid Mo(CO)<sub>6</sub>. With increasing substrate temperature, this valence band emission moves

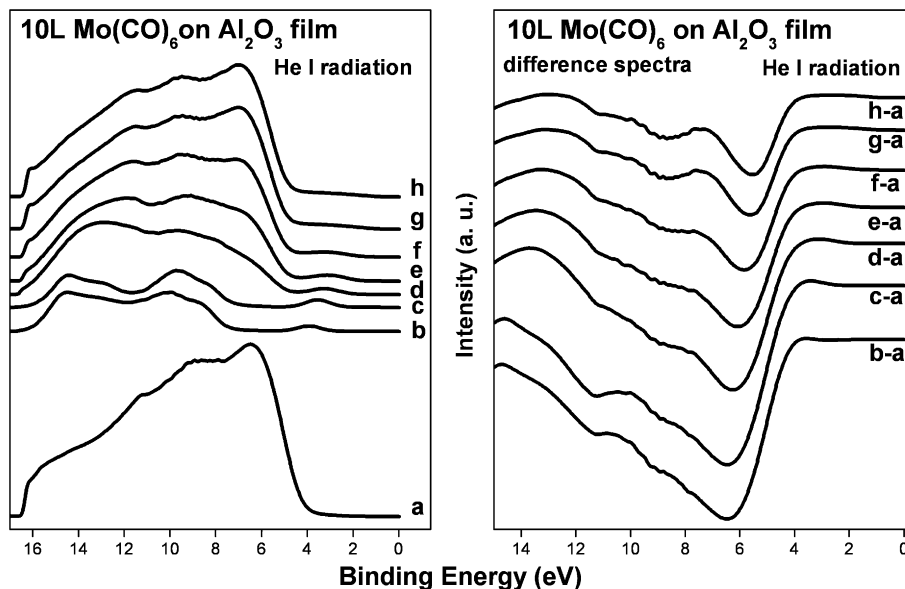


Fig. 7. UPS of  $\text{Mo}(\text{CO})_6$  adsorbed on the thin  $\text{Al}_2\text{O}_3$  film, (a) a clean  $\text{Al}_2\text{O}_3$  film; After dose of 10 L  $\text{Mo}(\text{CO})_6$  on the  $\text{Al}_2\text{O}_3$  film at 100 K, the sample was annealed at (b) 100 K, (c) 150 K, (d) 200 K, (e) 250 K, (f) 300 K, (g) 400 K, (h) 500 K. The difference spectra were obtained by subtracting the spectrum on the surface annealed at the indicated temperatures from the initial spectrum (a) of the clean  $\text{Al}_2\text{O}_3$  film.

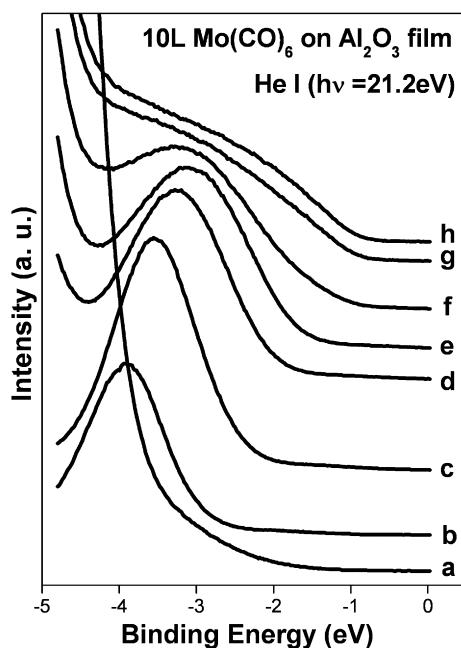


Fig. 8. UPS of  $\text{Mo}(\text{CO})_6$  adsorbed on the thin  $\text{Al}_2\text{O}_3$  film, (a) a clean  $\text{Al}_2\text{O}_3$  film; After dose of 10 L  $\text{Mo}(\text{CO})_6$  on the  $\text{Al}_2\text{O}_3$  film at 100 K, the sample was annealed at (b) 100 K, (c) 150 K, (d) 200 K, (e) 250 K, (f) 300 K, (g) 400 K, (h) 500 K.

towards lower binding energy, and decreases the intensity monotonically. It indicates that gradual decarbonylation derived from thermal decomposition occurs on the molybdenum carbonyls, inducing the Mo 4d valence band feature to shift downward. When the sample was annealed at 400 K, no prominent peak is observed in the UPS, but only a broad protrusion. In a  $\text{Mo}(\text{CO})_6$  molecule, the metal is surrounded by six CO ligands, constructing an octahedral

configuration. The valence electrons in the molybdenum are highly discrete, consequently exhibiting a sharp peak in the valence band region. After decarbonylation, upon annealing the molybdenum particles form on the oxide film, and the energy level grows continuously. The appearance of electronic band dispersion is a significant indication that the electrons are delocalized within the molybdenum and that the metallic molybdenum has formed.

Further increasing sample temperature, the metallic molybdenum particles undergo migration and agglomeration, and hence the 4d feature becomes wider and the centroid moves towards lower binding energy. Valence band narrowing and a shifting of the core lines towards higher binding energies with decreasing cluster size were generally observed. The former was considered to be an initial-state effect, and was commonly used to characterize the non-metal to metal transition of the clusters, whereas the latter was assigned in most cases to a final-state effect dominated by the Coulomb interaction induced by the charge left on the clusters following the emission of photoelectrons [52].

#### 4. Conclusions

The thin alumina film was prepared by deposition and oxidation of aluminum on a refractory  $\text{Re}(0001)$  substrate in a UHV system. The oxide film is long-range ordered, essentially stoichiometric and free from surface hydroxyl groups. XPS and UPS results reveal that  $\text{Mo}(\text{CO})_6$  adsorbs molecularly on the oxide film at 100 K; however, the adsorbate undergoes decarbonylation upon annealing at high temperatures. The metallic molybdenum clusters form on the thin alumina film after thermal decomposition of  $\text{Mo}(\text{CO})_6$ .

## Acknowledgement

This work was financially supported by the National Natural Science Foundation of China (90206036).

## References

- [1] R. Psaro, S. Recchia, *Catal. Today* 41 (1998) 139.
- [2] R.L. Banks, G.C. Bailey, *Ind. Eng. Chem. Prod. Res. Dev.* 3 (1964) 170.
- [3] A. Brenner, *J. Mol. Catal.* 5 (1979) 157.
- [4] E. Davie, D.A. Whan, C. Kemball, *J. Catal.* 24 (1972) 272.
- [5] J. Smith, R.F. Howe, D.A. Whan, *J. Catal.* 34 (1974) 191.
- [6] R. Thomas, J.A. Moulijn, *J. Mol. Catal.* 15 (1982) 157.
- [7] R.-I. Nakamura, R.G. Bowman, R.L. Burwell, *J. Am. Chem. Soc.* 103 (1981) 673.
- [8] A. Brenner, R.L. Burwell, *J. Catal.* 52 (1978) 353.
- [9] R.-I. Nakamura, D. Pioch, R.G. Bowman, R.L. Burwell, *J. Catal.* 93 (1985) 388.
- [10] J.-S. Chung, R.L. Burwell Jr., *J. Catal.* 116 (1989) 519.
- [11] M. Kaltchev, W.T. Tysoe, *J. Catal.* 193 (2000) 29.
- [12] M. Kaltchev, W.T. Tysoe, *J. Catal.* 196 (2000) 40.
- [13] M. Kaltchev, W.T. Tysoe, *Top. Catal.* 13 (2000) 121.
- [14] Y. Wang, F. Gao, M. Kaltchev, D. Stacchiola, W.T. Tysoe, *Catal. Lett.* 91 (2003) 83.
- [15] Y. Wang, F. Gao, M. Kaltchev, W.T. Tysoe, *J. Mol. Catal. A* 209 (2004) 135.
- [16] Y. Wang, F. Gao, W.T. Tysoe, *J. Mol. Catal. A* 235 (2005) 173.
- [17] Y. Wang, F. Gao, W.T. Tysoe, *J. Mol. Catal. A* 236 (2005) 18.
- [18] Y. Wang, F. Gao, W.T. Tysoe, *J. Mol. Catal. A* 248 (2006) 32.
- [19] Z.Q. Jiang, W.X. Huang, J. Jiao, H. Zhao, D.L. Tan, R.S. Zhai, X.H. Bao, *Appl. Surf. Sci.* 229 (2004) 43.
- [20] Z.Q. Jiang, W.X. Huang, Z. Zhang, H. Zhao, D.L. Tan, X.H. Bao, *J. Phys. Chem. B*, in press, doi:10.1021/jp065293i.
- [21] Z.Q. Jiang, H. Zhao, D.L. Tan, R.S. Zhai, X.H. Bao, *Chin. J. Catal.* 26 (2005) 423.
- [22] Y.T. Wu, E. Garfunkel, T.E. Madey, *J. Vac. Sci. Technol. A* 14 (1996) 2554.
- [23] F.R. de Boer, R. Boom, W.C.M. Mattens, A.R. Miedema, A.K. Niessen, *Cohesion in Metals*, North-Holland, Amsterdam, 1988.
- [24] D.R. Lide, *CRC Handbook of Chemistry and Physics*, 86th ed., CRC Press, Boca Raton, FL, 2005.
- [25] M.B. Lee, J.H. Lee, B.G. Frederick, N.V. Richardson, *Surf. Sci.* 448 (2000) L207.
- [26] B.G. Frederick, G. Apai, T.N. Rhodin, *Phys. Rev. B* 44 (1991) 1880.
- [27] M.-C. Wu, D.W. Goodman, *J. Phys. Chem.* 98 (1994) 9874.
- [28] R. Ducros, M. Alnot, J.J. Ehrhardt, M. Housley, G. Piquard, A. Cassuto, *Surf. Sci.* 94 (1980) 154.
- [29] J.A. Tossell, *J. Phys. Chem. Solids* 36 (1975) 1273.
- [30] A. Bianconi, R.Z. Bachrach, S.B.M. Hagstrom, S.A. Flodström, *Phys. Rev. B* 19 (1979) 2837.
- [31] A. Jimenez-González, D. Schmeisser, *Surf. Sci.* 250 (1991) 59.
- [32] P.C. Snijders, L.P.H. Jeurgens, W.G. Sloof, *Surf. Sci.* 496 (2002) 97.
- [33] B.G. Frederick, G. Apai, T.N. Rhodin, *Surf. Sci.* 244 (1991) 67.
- [34] M. Liehr, P.A. Thiry, J.J. Pireaux, R. Caudano, *J. Vac. Sci. Technol. A* 2 (1984) 1079.
- [35] L.H. Jones, *J. Chem. Phys.* 36 (1962) 2375.
- [36] L.H. Jones, *Spectrochim. Acta* 19 (1963) 329.
- [37] L.H. Jones, R.S. McDowell, M. Goldblatt, *Inorg. Chem.* 8 (1969) 2349.
- [38] T.A. Germer, W. Ho, *J. Chem. Phys.* 89 (1989) 562.
- [39] Z.C. Ying, W. Ho, *J. Chem. Phys.* 93 (1990) 9077.
- [40] S.K. So, W. Ho, *J. Chem. Phys.* 95 (1991) 656.
- [41] C.C. Cho, S.L. Bernasek, *J. Vac. Sci. Technol. A* 5 (1987) 1088.
- [42] B. Domenichini, S. Pétigny, V. Blondeau-Patissier, A. Steinbrunn, S. Bourgeois, *Surf. Sci.* 468 (2000) 192.
- [43] A. Nilsson, N. Mårtensson, S. Svensson, L. Karlsson, D. Nordfors, U. Gelius, H. Ågren, *J. Chem. Phys.* 96 (1992) 8770.
- [44] J. Bustad, C. Enkvist, S. Lunell, H. Tillborg, A. Nilsson, S. Osborne, A. Sandell, N. Mårtensson, S. Svensson, *Chem. Phys.* 179 (1994) 303.
- [45] G.M. Bancroft, B.D. Boyd, D.K. Creber, *Inorg. Chem.* 17 (1978) 1008.
- [46] H.-J. Freund, F. Greuter, D. Heskett, E.W. Plummer, *Phys. Rev. B* 28 (1983) 1727.
- [47] A. Iverson, B.R. Russell, *Chem. Phys. Lett.* 6 (1970) 307.
- [48] E.W. Plummer, W.R. Salaneck, J.S. Miller, *Phys. Rev. B* 18 (1978) 1673.
- [49] G.D. Michels, G.D. Flesch, H.J. Svec, *Inorg. Chem.* 19 (1980) 479.
- [50] Z.C. Ying, W. Ho, *J. Chem. Phys.* 94 (1991) 5701.
- [51] U.R. Schöffel, H. Rauscher, R.J. Behm, *J. Appl. Phys.* 91 (2002) 2853.
- [52] Y.Q. Cai, A.M. Bradshaw, Q. Guo, D.W. Goodman, *Surf. Sci.* 399 (1998) L357.